ACS Synthetic Biology

pubs.acs.org/synthbio
Research Article

Tuning Ultrasensitivity in Genetic Logic Gates Using Antisense RNA Feedback

Published as part of ACS Synthetic Biology special issue "IWBDA 2023".

Nicolai Engelmann, Maik Molderings, and Heinz Koeppl*

Cite This: *ACS Synth. Biol.* 2025, 14, 1425−1436
Read Online

ACCESS | Metrics & More | Article Recommendations

ABSTRACT: Inverting genetic logic gates fueled by transcriptional repression is an established building block in genetic circuit design. Often, the gates' dose−response curves require large changes in dose to transition between logic ON and OFF states, potentially leading to logically indeterminate intermediate states when gates are connected. Additionally, leakage in the OFF state is a general concern, especially at the output stages of a circuit. This study explores the potential to improve inverting logic gates through the introduction of an additional sequestration reaction between the input and output chemical species of the gate. As a mechanism of study, we employ antisense RNAs (asRNAs) expressed alongside the mRNA (mRNA) of the logic gate within single transcripts. These asRNAs target mRNAs of adjacent gates and create additional feedback that supports the protein-mediated repression of the gates. Numerical and symbolic analysis indicates that the sequestration steepens the gate's dose−response curve, reduces leakage, and can potentially be used to adjust the location of logic transition. To leverage these effects, we demonstrate how design parameters can be tuned to obtain desired dose−response curves and outline how arbitrary combinational circuits can be assembled using the improved gates. Finally, we also discuss an implementation using split transcripts.

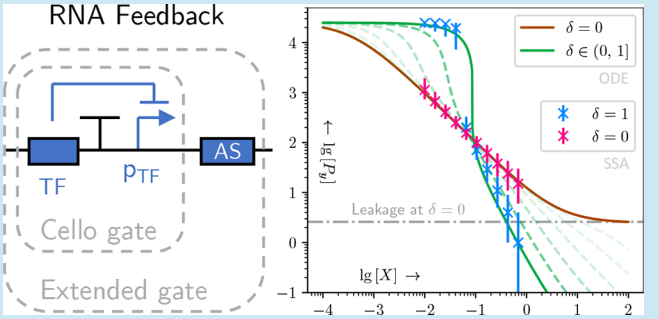

KEYWORDS: *synthetic biology, genetic circuit design, antisense RNA, feedback loop, ultrasensitivity, genetic design automation*

1. INTRODUCTION

The constituents of many cellular biochemical processes, such as the binding of regulator proteins to DNA binding-sites, appear to be related by dose−response curves that have sigmoid shape in a logarithmic argument.[1] This phenomenon has enabled synthetic biologists to engineer artificial genetic pathways that compute logic operations in vivo.[2] Competition for regulators by multiple binding domains, e.g., causing titration effects,[3] can increase or decrease the steepness of dose−response curves in the logarithmic domain.[4,5] Strong binding affinity to competing sites can effectively lead to a sequestration of regulators,[6] and it has been observed that this sequestration influences dose−response curves in a similar way.[7] Qualitative effects like this are of peak interest to researchers trying to engineer dose−response curves that behave like ideal logic switches.[8] At the same time, recent interest in computer-aided design (CAD) of complex genetic logic functions has raised demand for highly modular and reusable devices.[9] In Cello,[10,11] the most prominent of such CAD tools, logic computation is done by NOT and NOR gates only, implemented by proteins, specifically transcriptional repressors, and their corresponding promoters. Such protein-based circuits have been widely explored due to their ability to perform complex functions.[12]

In contrast, gene regulation in nature is not only mediated by proteins, but also by RNA molecules. They are produced and degraded more rapidly than proteins, allowing to propagate signals faster than their protein-based counter parts,[13] and impose significantly lower metabolic burden on the host. Several synthetic RNA switches have been developed and implemented in various organisms, showcasing the versatility and efficiency of RNA-based regulators.[14,15] Examples include small transcriptional activating RNAs (STAR),[16] toehold[17] and its eukaryotic version eToehold[18] switches. These RNA-based elements can control gene expression precisely and dynamically, often with higher specificity and lower energy requirements than their protein

Received: June 17, 2024
Revised: March 27, 2025
Accepted: March 31, 2025
Published: May 7, 2025

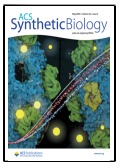

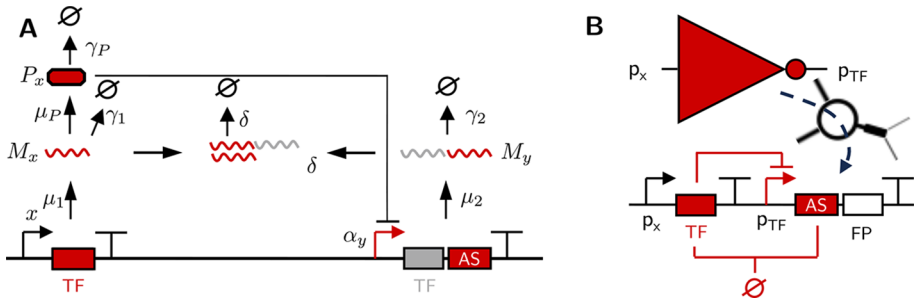

Figure 1. (A) Illustration of the proposed feedback architecture. Feedback is implemented through the transcription of RNA that includes both a coding and a noncoding segment. The coding segment is translated into a transcription factor, while the noncoding segment functions as an antisense RNA (asRNA) that targets the coding region of the input transcription factor. (B) Shows the SBOL diagram of an envisioned NOT gate with RNA-mediated feedback. The input species x is shown as a promoter activity and FP denotes a fluorescent protein as a potential output.

counterparts. In addition to these advances, another study demonstrated the integration of RNA regulation into a protein-based circuit, enabling fine-tuning of the protein gate's behavior.[19] Furthermore, a subsequent study explored this phenomenon in greater detail, employing various RNA regulatory strategies to achieve more nuanced control over the circuit's dynamics resulting in adaptive circuits.[20] RNA molecules also play natural regulatory roles within cells, as seen with long noncoding RNAs (lncRNAs)[21] and microRNAs (miRNAs)[22] in eukaryotes, which participate in intricate regulatory networks. In prokaryotes, RNAs also play a crucial role in gene regulation in the form of small RNAs (sRNAs) e.g., in controlling the global transcription factor Lrp in *E. coli*.[23] Another example is the control of low- and high-cell-density states in *Vibrio harveyi* by realization of negative feedback loops with luxO and luxR.[24] In this network, the sRNAs play a role in tuning the dynamic range of the quorum-sensing circuit. It is also proposed, that negative feedback plays a role in evolution by enhancing the robustness for mutations.[25] Noticeable is, that regulation by sRNA seems to have different characteristics than protein-mediated regulation.[26] This may explain why nature evolved into regulatory networks incorporating both protein and RNA mediated regulation, since they do not only regulate biological processes at distinct levels but also complement each other by compensating for their respective functional limitations, creating a synergistic interplay essential for cellular function. This natural predisposition for regulation makes RNA an attractive substrate for engineering synthetic feedback mechanisms within protein-based circuits. For instance, RNA-based integral feedback controllers using antisense RNA (asRNA) have been designed to maintain homeostasis within synthetic circuits, ensuring robust performance despite any perturbations of the system.[27] This asRNA has high target specificity and has wide usage in gene silencing in therapeutic applications.[28,29] In these applications, noncoding RNA (ncRNA) that is complementary to regions of the target mRNA acts as asRNA in transfected cells. The asRNA binds to the mRNA and forms double-strand RNA (dsRNA) that is either degraded by the host as a security measure, e.g., against viral attacks,[30] or forms a translationally inactive complex.

The goal of this work is to study the use of asRNAs to extend inverting protein-based genetic logic gates by a low-overhead feedback mechanism that aims to improve key characteristics of their dose−response curves, all while keeping their design modular as required by many genetic design automation tools.[9]

2. RESULTS

We use complementary RNA parts to mutually sequester RNA species adjacent to the TF-mediated transcriptional repression that constitutes the central part of an inverting logic gate. In this way, we effectively obtain a sequestration between the regulating and output species' of the inverting logic gate. Because the logic gate is inverting and the sequestration is mutual w.r.t. the regulating species of adjacent logic gates in a circuit, we expect an escalation of their input sensitivity and thus a steeper dose−response curve. Although we introduce a sequestration, the idea is somewhat comparable to that of a bistable toggle-switch,[2] and similar hurdles w.r.t. parameter tuning are to be expected.[31] In contrast to the toggle-switch, however, our approach can flexibly be configured due to RNA base-pairing implementing the sequestration.[32] We also expect a leakage-reduction due to the sequestration of leaking mRNA. Our method can be used on logic gates that have stricly inverting parts on the level of RNA[33−36] (NOT gates in[10] or NOR gates in[36]), but not on those that lack such parts (e.g., NOR gates in[10]).

In the following sections, we briefly describe the biochemical mechanism behind the RNA feedback architecture and propose an exemplary schematic layout for a simple NOT gate similar to those in.[10,36] Then, we investigate its impact on such a NOT gate by taking a look at its dose−response curve, for which we describe important qualitative properties and perform a quantitative study. We then provide a toolset to calibrate important kinetic parameters of the gate, and give an outlook on how such gates can be assembled together systematically to build arbitrary combinational logic circuits. Finally, we discuss a robust, alternative schematic layout.

2.1. RNA Feedback for Genetic Logic Gates. Many logic operations have been implemented in cells.[37] Among them, NOT and NOR gates are logic-complete, meaning they can be used to compute any logic operation.[38] These gates are simple to design using transcriptional repressors, which has led to their widespread adoption.[10,36] However, using only transcriptional repressors results in an on/off switch with a broad transition region, leading to variability where cells can be in a logically inconsistent state. Cells and organisms require switches that are distinctly on or off, with no intermediate states. To address this, nature has developed ultrasensitive switches.[39−41] Steep ultrasensitive switches can be achieved using different mechanisms: blocking, sequestration, and displacement.[42] Even though also transcriptional repressor-based switches show ultrasensitivity, they are limited in steepness due to the cooperativity which can be achieved.

https://doi.org/10.1021/acssynbio.4c00438
ACS Synth. Biol. 2025, 14, 1425−1436

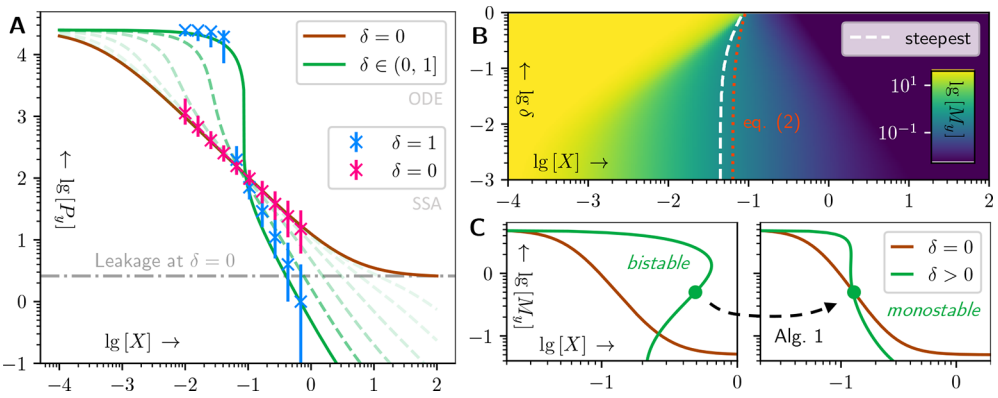

Figure 2. (A) Comparison of steady-state equations and stochastic simulation (SSA) of the exemplary NOT gate for different values of the sequestration rate δ (Methods 4.1). The SSA does not employ the QSS assumption from the RREs. Details are found in Methods 4.1.1. (B) Shows the narrowing transition region with increasing $\delta \in (0, 1]$ for the example NOT gate. The location of the steepest slope shifts in the process and the shape is no longer logistic. The reference location of the transition region x_{tr} from 2 is shown as a dotted red line. (C) Examplary usage of Alg. One for parameter tuning. The brown curves show the original dose−response. The green curves show steady-state curves (eq 12 from Methods 4.1.3) and the marker shows the transition location x_{tr} (eq 2). Random initialization of δ can lead to bistability, Alg. One finds the optimal translation and sequestration rates μ_P and δ (Methods 4.2).

RNA, feedbacking the translational process, adds minimal additional metabolic burden to the circuit.[16,43,44] We employ trans-acting asRNAs adjacent to the coding mRNA of a transcription factor (TF) in a single transcript. The start and stop codons surrounding the mRNA coding region ensure TF translation. The antisense region complements the coding region of the TF's transcript, as illustrated in Figure 1. Watson−Crick pairing forms double-stranded RNA (dsRNA), repressing translation due to RNA−RNA duplex degradation by various mechanisms in different hosts[45−47] or by blocking ribosome binding.[48] Somewhat complementary to the incoherent regulation through antithetic integral feedback,[27,49] we propose that coherent feedback mediation via sense and antisense RNA sequestration can enhance the function of genetic gates and circuits. As a design example, a transcriptional unit could be constructed with an asRNA region downstream of the protein-coding sequence. To optimize sequestration efficiency and specificity, varying lengths of the complementary parts should be tested to identify a design that ensures strong binding while minimizing off-target effects. Additionally, incorporating an HFQ binding site upstream of the antisense region may enhance the interaction between the asRNA and its target RNA, as HFQ is known to stabilize RNA−RNA interactions. In previous work, a similar feedback mechanism was achieved by fusing the coding region of a protein to a gRNA site, enabling feedback on an input promoter.[50]

2.2. NOT Gate. In this section, the NOT gate − the most simple inverting logic element that can be extended by the RNA feedback connection − is considered. An SBOL-type diagram of the NOT gate is shown in Figure 1B. It shares its structure with the NOT gate[51] used in Cello[10,11,36] with an additional asRNA as part of the transcript of the output chemical species. In the following, we analyze important features of the deterministic steady-state derived from the gate's reaction rate equations and the given parameters of the original NOT gate without feedback.

2.2.1. Steady-State Equations. Consider the reaction network of the simple NOT gate with feedback illustrated in Figure 1A. It shows an arbitrary input species X that modifies the transcription rate of an RNA M_x, which is then translated to protein P_x. This protein acts as a repressing TF on the promoter that enables transcription of RNA M_y. The quantity α_y denotes the promoter activity. M_x and M_y contain the matching sense and antisense regions that lead to dsRNA formation and thus inactivation/degradation which we model by a sequestration reaction. Small letters denote concentrations, e.g., $x \equiv [X]$ in the following. Note that while x will most often represent the promoter activity of an input promoter to the gate taking values in a finite range, we can always multiply the RNA rate constant μ_1 by a an arbitrary constant to rescale x. It thus makes sense for the scope of our analysis to work with a general input species $x \geq 0$. If not otherwise noted, we also generally assume a normalized reaction volume. The network's reaction rate equations (RREs) are derived in Methods 4.1.2 using a quasi-steady state (QSS) assumption on the association and dissociation events of the TF P_x at the binding sites of the promoter. This simply allows us to treat α_y as a black-box Hill-function provided by the corresponding equation of the existing NOT gate. Note that this is a common simplifying assumption.[52] The steady-state equations can then be given by

$$m_x = \frac{\mu_1 x}{\gamma_1 + \delta m_y}\alpha_y = \frac{\kappa^n(1-\beta)}{\kappa^n + (r_x m_x)^n} + \beta m_y = \frac{\mu_2 \alpha_y}{\gamma_2 + \delta m_x} \tag{1}$$

where $\beta \in [0, 1)$ determines the amount of leakage, $r_x \equiv \gamma_P^{-1}\mu_P$ is a coefficient that generally depends on the inverter circuit used, and n is a Hill coefficient. Finding an explicit closed-form expression for α_y or m_y in x is not possible in the general case because of the feedback connection. However, numerical evaluation is possible, e.g., using a fixed-point iteration on 1 or solving a root-finding problem. These methods also scale to circuits of many gates with potential feedback connections.[6]

2.2.2. Limiting Behavior and Leakage Reduction. Maximal gene expression is reached for $x = 0$. Then, 1 suggests that $m_x = 0$, $p_x = 0$ and so $\alpha_y = 1$ and in turn $m_y = \frac{\mu_2}{\gamma_2}$. For the minimal expression limit, we let $x \to \infty$ and assume $m_y < \infty$ stays finite. Then, $m_x \to \infty$ becomes infinite and as a consequence $\alpha_y \to \beta$. Hence, the concentration of the output RNA

https://doi.org/10.1021/acssynbio.4c00438
ACS Synth. Biol. 2025, 14, 1425−1436

$m_y = \lim_{m_x \to \infty} \frac{\mu_2 \beta}{\gamma_2 + \delta m_x} = 0$ goes to zero. Clearly, x will be bounded in a realistic setting. However, in contrast to the original NOT gate with $\delta = 0$, the steady-state leakage does not approach a constant asymptote for for $\delta > 0$ with increasing x. This can be seen in Figure 2C. Interestingly, a larger δ does not change the slope of the *asymptotic* decrease in m_y in a doubly logarithmic plot. This effect is not visible in Figure 2C, but it comes from the circumstance that the promoter activity α_y saturates, while m_y has a hyperbolic relationship with m_x via the feedback. Assume δ and x large. Then, $m_x \approx \frac{\mu_1}{\gamma_1} x$ and $\alpha_y \approx \beta$, and in turn $m_y \approx \frac{\gamma_1 \mu_2 \beta}{\delta \mu_1 x}$. This is equivalent to $\ln(m_y) \approx -\ln(x) + \ln\left(\frac{\gamma_1 \mu_2 \beta}{\delta \mu_1}\right)$. However, the point at which this asymptotic regime is reached varies with the value of δ, depending on when $\gamma_1\gamma_2 + \delta\mu_1 x \approx \delta\mu_1 x$ becomes valid. Note that it is likely that in a real-world setting, a saturation of the leakage reduction by the feedback can occur not only due to the limited range of x, but also due to transport limitations[53] or additional cellular mechanisms. However, it is reasonable to assume that a reduction can be achieved to some degree.

2.2.3. Location and Uniqueness of the Logic Transition Region. The logic transition region, or simply the transition region, is a term from electrical engineering that denotes the region of a dose−response curve, in which the change between qualitatively distinct states mainly occurs.[54] In a Hill-shaped dose−response curve, the transition region corresponds to the region around the inflection point, where the response changes rapidly with a change in dose. In this work, when we refer to the *location* of the transition region, we mean a specific reference dose that is deemed representative to the region. In a Hill-shaped dose−response curve, this could e.g., correspond to the dose at the inflection point.

In our NOT gate, the transition region in m_y becomes steeper the larger δ becomes, but also changes its location gradually with an increase in δ (c.f. Figure 2B). The input species concentration x that causes the largest change in m_y can e.g., be found numerically from 1, iterating over x. However, locating the transition region by this criterion makes most sense when the dose−response curve is given by a Hill function because of its logistic shape in the logarithmic domain. This shape, however, is lost with $\delta > 0$ and the dose−response curve exhibits no obvious symmetry. At the same time, the inflection point in the original Hill-shaped dose−response curve also corresponds to the input x, where the response has been attenuated by half the logarithmic difference between maximum and minimum response levels $\ln(m_{y,\max})$ and $\ln(m_{y,\min})$.

To obtain a useful criterion for all choices of $\delta \geq 0$, we set the reference response level m_{tr} for the transition region to this value, i.e., $m_{tr} \equiv \frac{1}{2}(\ln(m_{y,\max}) - \ln(m_{y,\min})) = \frac{\mu_2}{\gamma_2}\sqrt{\beta}$, where $m_{y,\max}$ and $m_{y,\min}$ are the corresponding values of the original NOT case $\delta = 0$. We can relate this choice to the concept of a threshold voltage in electronic logic gates.[54] In Methods 4.1.3, we show that the input x_{tr} corresponding to m_{tr} can be obtained as the root-finding problem

$$d_{n+1} x_{tr}^{n+1} + d_n x_{tr}^n + d_1 x_{tr} - d_0 = 0 \tag{2}$$

with the coefficients $d_0 = (1 - \sqrt{\beta})^2 \gamma_2 \kappa^n$, $d_1 \equiv \kappa^n \beta \delta c_1$, $d_n \equiv (r_x c_1)^n (1 - \beta)\beta\gamma_2$, $d_{n+1} = (r_x c_1)^n \beta \delta c_1$, where we introduced the additional constant $c_1 = \frac{\mu_1 \gamma_2}{\gamma_1\gamma_2 + \delta\mu_2\sqrt{\beta}}$. Because $\beta \in [0, 1]$, all coefficients are non-negative. Note that the power n is not necessarily an integer. Eq 2 has been obtained by insertion of m_{tr} into the equation system 1 and subsequent elimination of m_x and α_y. This does not lead to a loss of possible solutions for x_{tr}, because given $m_y = m_{tr}$, all equations in 1 are bijective in the remaining variables. Not only does 2 preserve all solutions, it has a unique non-negative real solution x_{tr} which we show in Methods 4.1.3. We plot x_{tr} as a function of δ for the example NOT gate in Figure 2B as a red dotted line.

As a more general case, we also show in Methods 4.1.3 that there even exists a unique non-negative real input x_{lv} for any arbitrary $m_{lv} \in [m_{y,\min}, m_{y,\max}]$. This has the consequence that the extended NOT gate has a unique transition region in the important range $[m_{y,\min}, m_{y,\max}]$. We expect the dose−response curve w.r.t. m_y (and in consequence a_y) to be monotonically decreasing with increasing x starting from an initial stable pair x', m_y', but a detailed analysis of this property is left open for future study.

Note that we can have multiple m_{tr} that result in the same solution x_{tr} in 2, so that multiple steady-states of 1 can exist. Given the regulatory motifs in our construct, we can expect 1 to exhibit bistability for certain values of δ. While bistability of the dose−response curve akin to that of a bistable toggle-switch[2] or a Schmitt trigger[55] is not necessarily an unwanted effect in a switch, we show how to calibrate the sequestration rate δ to avoid this effect entirely in section.

2.3. Tuning Design Parameters. An existing NOT gate that is extended by the RNA feedback mechanism can exhibit a shift in its transition location and potentially loose its monostability. The latter effect can be desirable, as the presence of a hysteresis imposes a stabilizing effect on the set logic levels in the presence of fluctuations of the gate's input. Still, a typical application would require most characteristic features of the original dose−response curve to stay unaltered, so that only its steepness increases and leakage decreases. At the same time, adjustments of design parameters to reach this goal must focus on those parameters that can be calibrated rather flexibly in the actual genetic design.

2.3.1. Calibration of the Transition Location. Modification of the transition location x_{tr} can be done by changing the scaling coefficient $r_x \equiv \gamma_P^{-1}\mu_P$ that controls the protein concentration $[P_x]$. Tuning the translation efficiency of P_x e.g., by choosing an appropriate Kozak sequence or RBS, depending on the organism, implements the change in r_x. Unfortunately, although r_x only appears in the equation for α_y in 1, it cannot simply be scaled by a factor $\hat{x}_{tr}/x_{tr}$ with the desired transition location $\hat{x}_{tr}$ due to the feedback. However, the adjusted scaling coefficient $\hat{r}_x$ corresponding to the transition location $\hat{x}_{tr}$ can be calculated explicitly by

$$\hat{r}_x = \frac{\kappa}{c_1 \hat{x}_{tr}} \left[1 - \frac{(1 - \sqrt{\beta})^2 \gamma_2}{\sqrt{\beta}\delta c_1 \hat{x}_{tr} + (1 - \sqrt{\beta})\gamma_2}\right]^{-1/n} \tag{3}$$

with the constant $c_1 \equiv \frac{\mu_1\gamma_2}{\gamma_1\gamma_2 + \delta\mu_2\sqrt{\beta}}$. eq 3 can be obtained by rearranging (2) under knowledge that $\hat{x}_{tr}$ is unique.

2.3.2. Preservation of Monostability. Monostability can be preserved by adjusting the sequestration rate δ. At the same time, δ can be tuned flexibly by modification of the free binding energy[56] between the engineered asRNA and its targeted mRNA. However, δ also determines the increase in

https://doi.org/10.1021/acssynbio.4c00438
ACS Synth. Biol. 2025, 14, 1425−1436

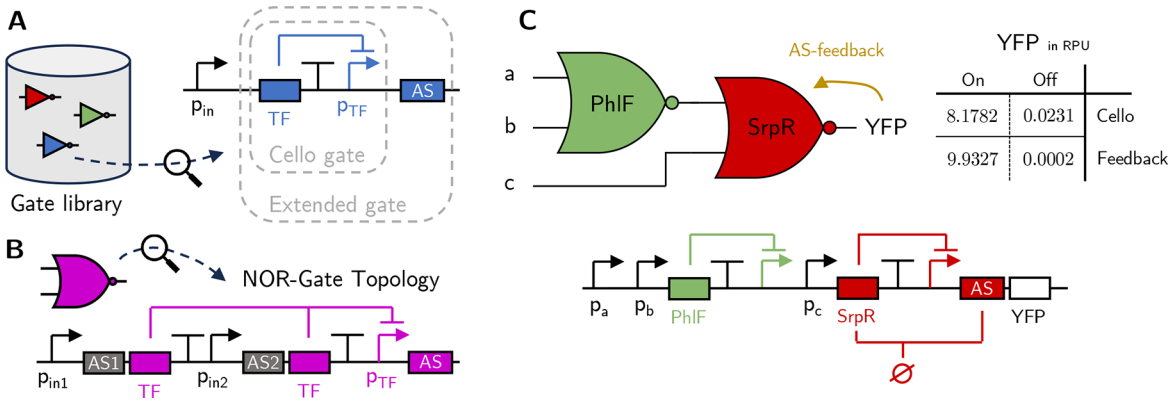

Figure 3. Construction of the NOR-logic circuit with RNA feedback. (A) Genetic parts can be organized in a gate library. Compared to Cello's gates, the extended gates contain an additional corresponding asRNA sequence that is placed next to the coding sequence of the output species. (B) NOR gates can be assembled in accordance to the logic function using the strategy in,[36] so that no mRNA is accidentally targeted that should exhibit a high copy-number. (C) Cello circuit 0 × 70 with optimal gate assignment and RNA-feedback from YFP to SrpR; the table shows the lowest ON and highest OFF concentrations of YFP. We stress that this is an in silico experiment under the model assumptions made in this work.

steepness of the dose−response curve. Thus, a desirable δ would be as large as possible without causing multistability. To achieve this, we again consider 2 from section. We have shown in 4.1.3 that the LHS of 2 describes a function $f(x, m_{\mathrm{lv}}) \in \mathbb{R}$ that is strictly monotonically increasing in $x \in (0, \infty)$ for constant m_{lv}. Assume now, we have determined a root x_{lv} that satisfies $f(x_{\mathrm{lv}}, m_{\mathrm{lv}}) = 0$ for a specific m_{lv}. Remember that a monostable inhibitory dose−response curve is stricly monotonically decreasing in m_{lv} for increasing x_{lv}. Thus, its inverse function is strictly monotonically decreasing in x_{lv} for increasing m_{lv} in its appropriate range. We must therefore demand for any $m_{\mathrm{lv}}' > m_{\mathrm{lv}}$ that the corresponding $x_{\mathrm{lv}}' < x_{\mathrm{lv}}$ is smaller if both $f(x_{\mathrm{lv}}', m_{\mathrm{lv}}') = f(x_{\mathrm{lv}}, m_{\mathrm{lv}}) = 0$. Now combining this with the monotonicity of $f(x, m_{\mathrm{lv}})$ in x for any given m_{lv}, we must demand that $\frac{\partial}{\partial m_y} f(x_{\mathrm{lv}}, m_y)|_{m_y = m_{\mathrm{lv}}} > 0$ for any pair $(x_{\mathrm{lv}}, m_{\mathrm{lv}})$ that satisfies $f(x_{\mathrm{lv}}, m_{\mathrm{lv}}) = 0$.

This condition is hard to guarantee for all pairs $(x_{\mathrm{lv}}, m_{\mathrm{lv}})$. However, we can exploit the fact that the reference point for the transition location $(x_{\mathrm{tr}}, m_{\mathrm{tr}})$ conveniently lies in proximity to the presumed center of the region, where multistability may occur. We can thus propose the following heuristic that should yield satisfying results in most realistic cases: a good choice for δ is one, in which $0 < \frac{\partial}{\partial m_y} f(x_{\mathrm{tr}}, m_y)|_{m_y = m_{\mathrm{tr}}} \ll 1$ is satisfied. Note that this partial derivative can be evaluated easily using automatic differentiators.

2.3.3. Combination of Both—Algorithmic Calibration of Parameters. Adjustment of the transition location and maintaining monostability is not as straightforward as simply applying the corrections from sections and 2.3.2 one after another. Every change in δ causes the transition location x_{tr} to change and every adjustment of r_x reweighs the contributions of transcriptional repression and sequestration to the shape of the dose−response curve. However, it is possible to use an iterative approach to jointly calibrate δ and r_x. An example algorithm that implements such an approach is given in Alg. One in Methods 4.2. We used Alg. One to find the optimal r_x and δ for the case shown in Figure 2C, where δ has been initialized to a value that caused bistability and a significant shift in transition location. Using Alg. 1, we shifted the transition location back to its original value and chose a δ that was close to its largest possible value in the monostable regime. The initial and terminal parameters are given in Methods 4.2.

2.4. Logic Circuit with RNA Feedback. In this section, we consider a full logic circuit whose gates are extended by RNA feedback. First, we investigate how an arbitrary existing gate architecture can be extended by RNA feedback and under which conditions. Second, we formally describe the full logic circuit with extended gates and present its steady-state equations.

2.4.1. RNA Feedback Can Extend Gates with Molecular NOR Logic. Many genetic gate architectures are composed of multiple parts that together implement the desired overall logic function. Given an existing architecture, a natural question to ask is how to properly integrate the RNA feedback mechanism in the architecture to obtain the desired effects and without disrupting the logic function. As an example, we can take a look at the NOR logic gates from.[36] This specific gate architecture together with an extension by the RNA feedback is shown in Figure 3B. Note that the architecture in[36] uses gene copies with individual promoters instead of the tandem promoter architecture in.[10] The latter is not compatible with the RNA feedback mechanism. This will be made clear in the following.

Mutual repression of translation between species of logic gates can impact their logic function. Therefore, a gate with multiple inputs logically consistent with the single-transcript RNA feedback connection must implement a generalized inverter structure on the *molecular* level. Let $O \in \{0, 1\}$ be the Boolean output of an N-input logic gate and $I_n \in \{0, 1\}$ for $n \in \mathcal{I} \subset \mathbb{N}$ its enumerated Boolean inputs. Let $\mathcal{T} \subset \mathcal{I}$ be the indices of the inputs targeted by RNA feedback. For the RNA feedback to work as intended, we must ensure that $O = \sum_{n \in \mathcal{T}} I_n$, i.e., the logic gate's output must be inverse to every input targeted by RNA feedback. Hence, because inversion is unambiguous in a Boolean setting, $\sum_{n \in \mathcal{T}} I_n$ fully determines the output O's value. As a consequence, any other inputs $n' \in \mathcal{I}$ with $n' \notin \mathcal{T}$, i.e., inputs that are not targeted by RNA feedback, necessarily become do not care, i.e., they have no influence on O's value. Removing the inputs that are do not care, the part extended by the RNA feedback must thus be logically inverting, i.e., implement NOR logic on the level of RNA. Consider again the gate architecture from[36] in Figure

https://doi.org/10.1021/acssynbio.4c00438
ACS Synth. Biol. 2025, 14, 1425−1436

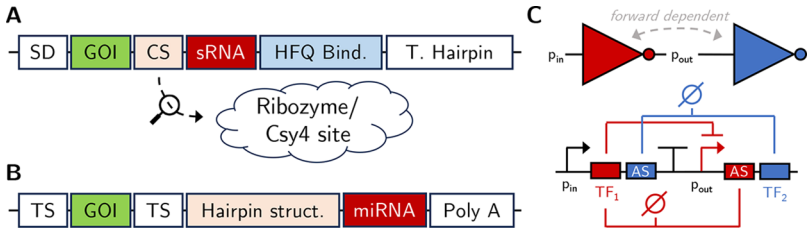

Figure 4. (A) Prokaryotic Design: This design features an RNA transcript that could be expressed in prokaryotes. The coding region includes the gene of interest (GOI), which may encode a transcription factor or fluorescent protein, preceded by the Shine-Dalgarno sequence (SD) as part of the translation initiation region. The noncoding portion of the transcript is cleaved by a Csy4 site or a self-cleaving ribozyme and contains a small RNA (sRNA) targeting the input or output protein of the gate. This region also includes an HFQ binding site to enhance repression efficiency. A strong terminator hairpin at the transcript's end ensures the correct folding of the HFQ binding site by mitigating readthrough. (B) Eukaryotic Design: Similar to the prokaryotic design, the eukaryotic RNA transcript comprises coding and noncoding regions. The GOI is flanked by miRNA target sites (TS), enabling regulation through miRNA activity. To stabilize the mRNA after miRNA excision by Dicer proteins, a stabilizing hairpin structure is included. This design mirrors the modularity of the prokaryotic system while adapting to eukaryotic cellular machinery. (C) Simplified SBOL-type diagram for the NOT gate using the split-transcript approach.

3B. There, the logically inverting part is the repression of the transcript that carries the mRNA of the internal TF of the gate by a previous gate's TF. Because each previous gate's TF represses a promoter that is placed upstream of an individual copy of the internal TF's gene, we can express a combinational circuit with this gate architecture as a tree of elementary OR and NOT gates on the molecular level (RNA or Protein) by associating each species with the individual gene copy it originates from. Inclusion of the RNA feedback is then viable. Using a single gene driven by a tandem promoter instead does not allow such a decomposition on the molecular level and our logic requirement $O = \overline{\sum_{n\in\mathcal{T}} I_n}$ cannot be satisfied. This prohibits the use of our RNA feedback in the NOR gates from,[10] but allows its use for those from.[36]

2.4.2. RNA-Feedback NOR-Logic Circuit. Let the topology of a NOR-logic circuit be a directed graph $\mathcal{G}\equiv(\mathcal{V}, \mathcal{E})$, where the vertices (gates, inputs or outputs) $\mathcal{V}\equiv\{v_1, \cdots, v_K\}$ are enumerated by the totally ordered index set $\mathcal{K}\equiv\{1, \cdots, K\}$. The set $\mathcal{E} \subset \mathcal{V} \times \mathcal{V}$ of directed edges (i.e., wires) in conjunction with the enumeration $\mathcal{K}$ lets us define incoming $\mathcal{I}_k\equiv\{m|(v_m \to v_k) \in \mathcal{E}, m \in \mathcal{I}\}$ and outgoing $\mathcal{O}_k\equiv\{m|(v_k \to v_m) \in \mathcal{E}, m \in \mathcal{I}\}$ index sets each for vertex v_k. We also define input $\mathcal{U} \subset \mathcal{I}$ and output $\mathcal{Y} \subset \mathcal{I}$ index sets for the whole circuit. While the topology $\mathcal{G}$ is obtained in the logic synthesis step of the automated design pipeline, the technology mapping step introduces an injective labeling function M: $\mathcal{V} \to \mathcal{L}$ that maps each vertex to an element of a library $\mathcal{L}$, i.e., a set of gate parameters from a gate library. Let the mapped gate parameters $M(v_k) = (\mu_k, \gamma_k, \beta_k, \delta_k, n_k, \kappa_k, r_k) \in \mathcal{L}$ be known for each $k \in \mathcal{K}\backslash\mathcal{U}$. We then seek to determine the circuit response α_y for $y \in \mathcal{Y}$ for given fixed inputs α_u = const. for $u \in \mathcal{U}$. To achieve this, we need the gates' output promoter activities α_k for each gate k. To determine α_k, we further need the RNA concentrations $\forall\, l \in \mathcal{I}_k$: $m_{l\to k}$ associated with each input of the gate, i.e. each copy of gate k's gene. Note that in a NOR-logic circuit as in,[10] we have $|\mathcal{I}_k| \leq 2$ for any k. For convenience, we define the total RNA concentration of gene k as $m_k\equiv\sum_{l\in\mathcal{I}_k} m_{l\to k}$. Then, to obtain the circuit response α_y with fixed input α_u = const., we need to solve the set of fixed-point equations

$$\alpha_k = \frac{\kappa_k^{n_k}(1-\beta_k)}{\kappa_k^{n_k} + (r_k m_k)^{n_k}} + \beta_k,\ \forall\, l \in \mathcal{I}_k\colon m_{l\to k} = \frac{\mu_l \alpha_l}{\gamma_k + \delta_l m_l + \sum_{i\in O_k} \delta_k m_{k\to i}} \tag{4}$$

for each $k \in \mathcal{K}\backslash\mathcal{U}$. The calculated $m_y \propto [P_y]$ for each $y \in \mathcal{Y}$, proportional to concentrations of reporter proteins $[P_y]$, can then be used to score the circuit.[10,57]

2.4.3. Cello Circuit End-Stage Example. Translation to Cello's circuit framework faces several challenges. Cello's gates feature only parameters $\alpha_{\max,k}$, $\alpha_{\min,k}$, K_k and n_k. Matching the parameters from our NOT example in section is underdetermined and thus leads to ambiguities. However, we see that $\alpha_{\min,k} = \beta\alpha_{\max,k}$ and $\alpha_{\max,k} \propto \frac{\mu_k}{\gamma_k} r_k$ (with any $\delta = 0$ we have $p_k = r_k m_k = \frac{\mu_{P,k}\mu_k}{\gamma_{P,k}\gamma_k}\alpha_k$). Although oversimplifying, we can fix the degradation rates $\gamma_{P,k}$ and γ_k to values representing their "typical" order of magnitude for *E. coli* (in full knowledge that they may vary greatly in reality). We also set $\mu_{P,k} \equiv \omega_{P,k}$ and $\mu_{P,k} \equiv \alpha_{\max,k}\omega_k$ with the proportionality factors $\omega_{P,k}$ and ω_k representing "typical" orders of magnitude for translation and transcription rates. This unifies r_k for all gates and we finally set $\kappa = K_k r_k$. With this setup, we took circuit 0 × 70 from[10] and equipped our simulation engine[58] with equation system 4 to check how different the circuit behaved with $\delta_y = 1$ for the YFP end-stage. The comparison of the circuit's closest ON-OFF output pair in the configurations with and without feedback ($\delta_y = 1$ and $\delta_y = 0$) is given in Figure 3C. More details are found in Methods 4.3.

2.5. Thoughts on a Split-Transcript Approach. A related concept uses split-transcripts to implement the asRNA bypass connection (which then needs to be extended with an explicit forward connection). While this approach might carry some potential drawbacks regarding modularity and scalability for arbitrary genetic circuits, it can be useful in case the single transcripts become too long or structural problems arise. In this approach, a reaction is included that causes the single-transcript RNA to be cleaved (split) into two RNAs. One carries only the mRNA part, and the other carries only the asRNA part of the adjacent mRNA species. We briefly discuss the biology of this approach in the following and relate its quantitative features to our computations for the single-transcript approach.

https://doi.org/10.1021/acssynbio.4c00438
ACS Synth. Biol. 2025, 14, 1425−1436

In prokaryotes, a transcriptional unit typically consists of a promoter followed by a Shine-Dalgarno sequence, the start codon of a gene of interest (GOI), and a transcriptional termination signal. To incorporate an antisense RNA (asRNA) within the transcript, Figure 4A illustrates the addition of a cleaving sequence (CS), such as a self-cleaving ribozyme or a Csy4 stem loop, upstream of the GOI. This design results in two RNA molecules: one that is translated into the GOI and another that acts as a repressor by targeting the RNA of an upstream or downstream gene in the circuit, thereby realizing the feedback and/or feedforward mechanism. The strength of this repression can be fine-tuned by varying the length and degree of mismatches between the target RNA and the asRNA, as well as incorporating an HFQ binding motif to enhance repression efficiency. Established protocols for designing sRNAs are readily available.[56,59,60] If a second sRNA is required—for instance, to simultaneously regulate feedback and feedforward or to target both inputs of a NOR gate—an additional cleaving sequence can be introduced upstream of the HFQ binding site, enabling the formation of an sRNA array.

The eukaryotic realization shares structural similarities with the prokaryotic design but incorporates key differences. Figure 4B depicts a potential RNA transcript within a genetic circuit, where the GOI is flanked by miRNA target sites (TS).[61,62] These TS regions are designed to match the specific miRNA sequences intended for binding. Downstream of the GOI, a stabilizing hairpin structure can be included[63] to ensure proper mRNA stability following miRNA excision by Drosha.[64] This design leverages the modularity of RNA-based regulation while adapting it to eukaryotic cellular mechanisms.

In comparison to the simple NOT gate with the single-transcript feedback approach studied in Section 2.2, the reaction network that represents the NOT gate with split-transcript approach is significantly larger and more complicated. It not only loses the stoichiometric 1:1 correspondence between sequestered input and output mRNAs, but it also introduces (at least) four more species, which correspond to the partial RNAs generated by the cleavage of the input and output RNAs. However, under specific conditions, the calculations done for the single-transcript can be carried over to the split-transcript, and the steady state eq 1 hold. These conditions require a unification of the degradation rates of the partial RNAs and the equality of the backward and forward sequestration rates. An exemplary reaction network, the associated RREs, and a proof of correspondence for the steady state equations for this network under these conditions is found in Section 4.4.

3. DISCUSSION

In this work, we performed a qualitative and quantitative analysis of how an inclusion of a sequestration reaction between the chemical species of an inverting genetic logic gate could impact the dose−response curve of the gate. For this analysis, we chose an asRNA-mediated feedback as the mechanism that implements the sequestration. We pointed out, how the observed effects constitute improvements of the characteristics of the logic gate, that are an increase in steepness of the logic transition region and a reduction in leakage.

The increase in steepness cannot be achieved to an arbitrary degree overall, but numerical analysis has provided evidence that especially in the high-response regime immediately below the inflection point of the original Hill-shaped dose−response curve, strong sequestration can lead to almost vertical sections in the dose−response curve. This qualitative effect has previously been observed[7] and is here likely due to the dominance of the hyperbolic feedback term that effectively reduces the concentration of the input RNA and thus the repressing TF. However, as the low-response, high-dose regime is entered, the dose−response curve is dominated by transcriptional repression and the hyperbolic feedforward term, that continually reduce the concentration of output RNA with increasing input promoter activity and thus input RNA concentration.

With an increase in sequestration rate, the dose−response curve can lose injectivity and the logic gate can experience bistability. This effect can lead to a hysteresis in the dose−response curve which can be beneficial in stabilizing logic levels. This hysteresis must be finely calibrated though, as it becoming too strong can cause switching to become almost impossible and it can effectively widen the region in which logic transitions occur. In addition to that, in a genetic logic circuit that consists of a cascade of inverting logic gates, multistability must be very carefully integrated, especially because the logic levels within the circuit are instantiated nontrivially before an inducer is added. Thus, it can be crucial to maintain monostability, which is why we proposed Alg. One for parameter tuning.

Leakage reduction is important in many applications, and using RNA sequestration to achieve this is an established concept.[28,29] While our model predicts an arbitrarily strong leakage reduction, it certainly misses out on some effects. Those effects may include imperfect blocking of ribosome recruitment by dsRNA formation or spatially heterogeneous sequestration rates due to transport limitations of chemical species. However, especially in scenarios where the choice of possible inducible promoters is limited to such with significant leakage, addition of RNA feedback can be an easy way to achieve strong leakage reduction.

The RNA feedback mechanism can be readily adapted to existing logic gates that incorporate inverting logic elements between constituting chemical species, the simplest of those being NOT/NOR gates. Researchers and engineers can integrate this structure into both current and newly developed gates. Tuning gate characteristics to more closely resemble those of an ideal logic gate is important for switches that must avoid intermediate states, such as kill switches. Biosensors can also benefit, as they only need to detect the definite presence or absence of a compound. We gave an outlook on the integration of the RNA-feedback mechanism into genetic circuits with multiple gates. In genetic design automation, integrating RNA-mediated feedback into existing gate libraries is straightforward and can result in enhanced performance in circuits of any size. Circuit simulation and parameter tuning as part of the technology mapping process become more expensive, but time-frames and general cost of wetlab iteration still outweigh drylab computation cost and time by a large margin, justifying the additional expense to be made.

Both the single- and split-transcript approaches suffer from limitations that must be considered for an in vivo implementation. As mentioned in Sections 2.1 and 4.4, incorporating an HFQ binding site downstream of the antisense region may improve its binding efficiency to the target. However, this could result in HFQ competition, ultimately leading to growth defects.[65] A potential solution is

https://doi.org/10.1021/acssynbio.4c00438
ACS Synth. Biol. 2025, 14, 1425−1436

to modify HFQ expression levels,[60] although this approach requires careful optimization. Expressing the coding and antisense regions in a single transcript may also by itself pose challenges. A long transcript could fold in such a way that the antisense region or HFQ binding site becomes inaccessible to the target or the HFQ chaperone, respectively, rendering the antisense region nonfunctional. The split-transcript approach, while circumventing this issue, introduces its own limitations. For instance, expressing Csy4 for transcript cleavage adds metabolic burden to the host, potentially causing circuit failure. While ribozymes avoid this by not requiring protein expression, they can leave residual nucleotides on the 3′ end of the sRNA,[66] which may hinder proper binding to the target RNA. To our knowledge, expressing miRNAs and a coding gene within a single transcript has not yet been experimentally demonstrated. Therefore, the proposed design may require modifications to ensure functionality. For example, the triple hairpin structure used for mRNA stabilization was originally designed for exogenously delivered mRNAs,[63] and its compatibility with endogenously produced transcripts is uncertain. Further experimental validation is necessary to determine whether translation is feasible under these conditions. An alternative strategy involves expressing the sRNA and miRNA in separate transcriptional units. This can be achieved by mirroring the promoter driving the gate's protein, effectively mimicking the corresponding gate structure. However, this configuration introduces potential issues with transcriptional noise, which may lead to unequal expression levels of the protein's mRNA and the sRNA/miRNA. Such imbalances could result in unintended effects, necessitating careful evaluation to ensure consistent circuit behavior.

Finally, while the sequestration between chemical species of logic gates has been envisioned to happen in the form of asRNA targeting and dsRNA formation in this work, the specific way this sequestration is implemented is transparent in the theoretical analysis, and other means of implementation are imaginable. Even the use of protein−protein interactions, like inteins[67] or dimerization,[68] or RNA-protein interactions e.g., RNA-targeting Cas proteins,[69,70] to implement the sequestration would require only minor changes in the proposed equations and the qualitative statements made w.r.t. the affected species remain.

4. METHODS

4.1. Single NOT Gate Case Study. The parameters for the quantitative study of the single NOT gate presented were chosen to be $\mu_1 = 1$, $\mu_2 = 10$, $\gamma_1 = \gamma_2 = 0.2$, $\mu_p = 1$, $\gamma_p = 0.002$, $\beta = 10^{-4}$, $K = 1$ and $n = 1$. For the steady-state analysis using the ODEs, the free parameters x and δ were chosen to fall in the ranges $x \in [10^{-4}, 10^{2}]$ and $\delta \in [0, 1]$. The five dashed curves in Figure 2A correspond to $\delta \in \{0.001, 0.004, 0.016, 0.066, 0.27\}$. Note that the choice $\mu_1 = 1$ is somewhat arbitrary, because we chose x to be a generic input variable. The setup for the stochastic simulation is explained in the following.

4.1.1. Stochastic Simulation of the NOT Gate. The SSA simulation for the NOT gate studied in Section 2.2 consisted in total of 8 species and 14 reactions. The two promoters were modeled using a two-state switching leaky promoter model[71] comprising of two species X_{ON}, X_{OFF} and G_{ON}, G_{OFF} each with conservation laws $X_{ON} + X_{OFF} = G_{ON} + G_{OFF} = 1$. In our example, we restrict ourselves to a cooperativity index of one ($n = 1$), so that we can model the switching between G_{ON} and G_{OFF} by simple association−dissociation reactions. The reactions for the switching of the two promoters are then given as

$$X_{OFF} \xrightarrow{k_{x,ON}} X_{ON}G_{OFF} \xrightarrow{k_f} G_{ON} + P_x \tag{5}$$

$$X_{ON} \xrightarrow{k_{x,ON}} X_{OF}G_{ON} + P_x \xrightarrow{k_r} G_{OFF} \tag{6}$$

The switching rate constants k_f and k_r were chosen to be consistent with the desired parameters of the black-box (normalized) Hill function of the existing logic gate in 1 and match the time-scale of transcription and translation. Similarly, the switching rates $k_{x,ON}$, $k_{x,OFF}$ were chosen to be consistent with the configurable steady-state input promoter activity. The two RNA and two protein species' M_x, M_y and P_x, P_y are given modulated birth and death reactions of the form

$$X_{ON} \xrightarrow{\mu_1} X_{ON} + M_xG_{ON} \xrightarrow{\mu_2} G_{ON} + M_y \tag{7}$$

$$G_{OFF} \xrightarrow{\mu_{2,l}} G_{OFF} + M_yM_x + M_y \xrightarrow{\delta} \emptyset \tag{8}$$

$$M_x \xrightarrow{\gamma_1} \emptyset M_y \xrightarrow{\gamma_2} \emptyset \tag{9}$$

$$M_{x/y} \xrightarrow{\mu_p} M_{x/y} + P_{x/y}P_{x/y} \xrightarrow{\gamma_p} \emptyset \tag{10}$$

where the slash indicates the same reaction and rate constant is used for both subscripts. The simulations were performed for 10 different input promoter activities $x = k_{x,ON}(k_{x,ON} + k_{x,OFF})^{-1}$ equally spaced in the log-domain in the interval $x \in [10^{-2}, 1]$. For each input promoter activity, 10,000 trajectories were drawn with sufficient length to reach a steady state. For each obtained steady-state empirical distributions, the median and the 0.1- and 0.9-quantiles were calculated and are shown using markers and errorbars in Figure 2C.

4.1.2. Reaction Rate Equations and Steady State. To derive the reaction rate equations corresponding to the reactions in 5 and 7, we make a quasi-steady-state (QSS) assumption for the association and dissociation events of transcription factors to and from the promoters in the time-scale of transcription and translation.[52] Thus, we assume

$$x = \frac{k_{x,ON}}{k_{x,ON} + k_{x,OFF}}\alpha_y = \frac{\kappa^n(1-\beta)}{\kappa^n + (r_xm_x)^n} + \beta \tag{11}$$

at all times. Because the rate constants $k_{x,ON}$, $k_{x,OFF}$ can be freely chosen in this setting, we treat x as an independent variable from now on. The reaction rate equations for the remaining species are then given by

$$\frac{d}{dt}m_x = \mu_1 x - \gamma_1 m_x - \delta m_x m_y, \quad \frac{d}{dt}m_y = \mu_2\alpha_y - \gamma_2 m_y - \delta m_x m_y$$

$$\frac{d}{dt}p_x = \mu_p m_x - \gamma_1 p_x, \quad \frac{d}{dt}p_y = \mu_p m_y - \gamma_p p_y$$

Setting all time-derivatives to zero and rearranging the equations, we obtain the steady-state eq 1.

4.1.3. Uniqueness of the Transition Region. We have shown in Section 2.2 that the maximum output RNA concentration $m_{y,max}$ at $x = 0$ is the same for any choice of sequestration rate δ. While the minimum output RNA concentration $m_{y,min}$ for $x \to \infty$ is only nonzero in the case of $\delta = 0$. However, in the application context of a genetic logic

https://doi.org/10.1021/acssynbio.4c00438
ACS Synth. Biol. 2025, 14, 1425−1436

gate, it makes sense to ask for the point $x = x_{lv}$, where $m_y(x)$ as a function of x crosses a constant line $m_y(x_{lv}) = m_{lv}$ that lies in the feasible region of the original NOT gate without feedback, where $\delta = 0$, and how often it crosses it, i.e. how many solutions for x_{lv} we can find for a given m_{lv}. Using this rationale, we can not only make statements about the approximate location of the transition region of the extended NOT gate, but we can also determine whether there exist multiple transition regions due to the feedback connection with $\delta > 0$ − an undesired property for a logic gate. Consider the steady-state eq 1 from Section 2.2. Inserting m_{lv} into the equations for m_y and m_x, we get

$$m_{lv}\delta m_x + m_{lv}\gamma_2 = \mu_2\alpha_y m_x = \frac{\mu_1}{\gamma_1 + \delta m_{lv}}x = c_1 x$$

where we introduced the constant c_1 for convenience. We then insert the expression for α_y, substitute $m_x = c_1 x$ and rearrange to get

$$(\kappa^n + (r_x c_1)^n x^n)(m_{lv}\delta c_1 x + m_{lv}\gamma_2) = \mu_2\kappa^n(1-\beta) + (\kappa^n + (r_x c_1)^n x^n)\mu_2\beta$$

$$(\kappa^n + (r_x c_1)^n x^n)\left(m_{lv}\frac{\delta}{\gamma_2}c_1 x + m_{lv} - \frac{\mu_2}{\gamma_2}\beta\right) = \frac{\mu_2}{\gamma_2}\kappa^n(1-\beta)$$

where we divided everything by γ_2 in the last line. At this point, we can recognize $m_{y,\min} = \frac{\mu_2}{\gamma_2}\beta$ and $m_{y,\max} = \frac{\mu_2}{\gamma_2}$ from the original gate $\delta = 0$. We insert these and subtract both sides by $\kappa^n(m_{y,\max} - m_{y,\min})$ to get

$$\underbrace{\kappa^n m_{lv}\frac{\delta}{\gamma_2}c_1 x + (r_x c_1)^n\left(m_{lv}\frac{\delta}{\gamma_2}c_1 x^{n+1} + (m_{lv} - m_{y,\min})x^n\right)}_{\equiv g(x, m_{lv})} - \underbrace{\kappa^n(m_{y,\max} - m_{lv})}_{\equiv C(m_{lv})} = 0 \quad (12)$$

We combine the full LHS of 12 in a single function $f(x, m_{lv}) \equiv g(x, m_{lv}) - C(m_{lv})$. We can now make sense of this equation. If we consider only $m_{lv} \in [m_{y,\min}, m_{y,\max}]$, then not only $C(m_{lv}) \geq 0$, but also $g(0, m_{lv}) - C(m_{lv}) \leq 0$. At the same time, g is a (generalized) polynomial in x with only non-negative coefficients and thus constitutes a monotonically increasing function for $x \geq 0$, i.e. $\frac{d}{dx}f(x) \geq 0$. It is in fact strictly monotonically increasing, i.e. $\frac{d}{dx}f(x) > 0$, within the interior $x \in (0, \infty)$ and only violates strict monotonicity at the boundary $x = 0$ for the choice $m_{lv} = 0$. Hence, f is bijective in the region $x \geq 0$. Since f is also continuous in x and (formally) unbounded, $g(x, m_{lv})$ either has the solution $x = 0$ or changes sign once for $x \in (0, \infty)$. Thus, $g(x_{lv}, m_{lv}) = 0$ has a unique solution x_{lv} for any $m_{lv} \in [m_{y,\min}, m_{y,\max}]$. Thus, any concentration $m_{lv} \in [m_{y,\min}, m_{y,\max}]$ can only be reached from a unique dose x_{lv}.

4.1.4. Reference Location of the Transition Region. Asking for a single point of transition x^{tr} akin to the inflection point of a Hill-shaped dose−response curve might not be answered consistently in general, because the transition region becomes nonsymmetrical due to the feedback and is unbounded from below (as can be seen in the example in Figure 2C). However, it makes sense to rephrase the question slightly and ask, where the value $m_y = m_{tr}$ is reached for $\delta > 0$ that constitutes the inflection point of the original NOT gate, where $\delta = 0$. The inflection point of the original NOT gate is found at

$$m_{tr} = \exp\left(\frac{1}{2}(\ln(m_{y,\max}) + \ln(m_{y,\min}))\right) = \exp\left(\frac{1}{2}\left(\ln\left(\frac{\mu_2}{\gamma_2}\right) + \ln\left(\frac{\mu_2}{\gamma_2}\beta\right)\right)\right) = \frac{\mu_2}{\gamma_2}\sqrt{\beta}$$

Inserting this in eq 12 gives

$$\kappa^n\beta\delta c_1 x_{tr} + \beta(r_x c_1)^n(\delta c_1 x_{tr}^{n+1} + \gamma_2(1-\beta)x_{tr}^n) - \gamma_2\kappa^n(1-\sqrt{\beta})^2 = 0$$

Introduction of the coefficients $d_1 \equiv \kappa^n\beta\delta c_1$, $d_n \equiv \beta(r_x c_1)^n(1-\beta)\gamma_2$, $d_{n+1} = (r_x c_1)^n\beta\delta c_1$ and $d_0 = (1-\sqrt{\beta})^2\gamma_2\kappa^n$ gives eq 2 from Section 2.2.

Algorithm 1 Calibration of the Dose-Response Curve

Require: Parameters of the original NOT gate, initial δ, tolerances $\epsilon > 0$ and $\Delta > 0$

Set $\hat{r}_x \leftarrow \gamma_2^{-1}\mu_2$ and $\hat{\delta} \leftarrow \delta$
Set $x_{tr} \leftarrow (r_x\mu_1)^{-1}\kappa\gamma_1\sqrt[n]{[\sqrt{\beta}(1-\sqrt{\beta})]^{-1} - 1}$ ▷ *its original value*
Set $m_{tr} \leftarrow (\gamma_2)^{-1}\mu_2\sqrt{\beta}$
Set $g \equiv \frac{\partial}{\partial m_y}f$ ▷ *e.g. using autograd*
Set $x' \leftarrow x_{tr}$ and $h \leftarrow h_0$ ▷ *choose some initial step-size* h_0
while $g(x', m_{tr}) - \Delta > \epsilon$ **do**
  $\hat{\delta} \leftarrow \hat{\delta} + h\,(g(x', m_{tr}) - \Delta)$
  Set $\hat{r}_x \leftarrow (3)$ with current $\hat{\delta}$ and x_{tr}
  Set $x' \leftarrow$ (non-negative) root of (2)
  Update h ▷ *e.g. by an annealing schedule or not at all*
end while
Set $r_x \leftarrow \hat{r}_x$ and $\delta \leftarrow \hat{\delta}$

4.2. Parameter Tuning Algorithm and Example. We give an exemplary parameter tuning algorithm in Alg. 1. The common design parameters that generated the steady-state curves in the NOT gate example in Figure 2C are $\mu_1 = \mu_2 = 1$, $\gamma_1 = \gamma_2 = 0.2$, $r_x = 1$, $\beta = 10^{-2}$, $\kappa = 0.3$ and $n = 3$. In the monostable case, the dose−response curve coincides with the steady-state curve, and the varying parameters are r_x and δ. The vanilla NOT gate's curve, where there is no RNA feedback, is generated with $r_x = 1$ and $\delta = 0$. The green curve on the LHS of Figure 2C is generated with $r_x = 1$ and $\delta = 3$ and shows an S-shape typical for a bistable system like the bistable toggle-switch. Application of Alg. One then yields the new parameters $r_x \approx 1.22$ and $\delta = 0.138$ that generate the green curve on the RHS of Figure 2C, which is monostable and centered around the logarithmic inflection point of the original NOT gate's dose−response curve.

4.3. Circuit Simulation with Feedback Using ARCTIC. The circuit simulations in Section 4.3 are done using the circuit simulator of the CAD software ARCTIC.[58] ARCTIC uses a fixed-point algorithm to evaluate the circuit response of a logic circuit with feedback connections (that is not combinational) and supports array-valued quantities to be communicated between the logic gates. The latter feature was used to communicate RNA concentrations together with promoter activities between the gates. The simulation library devised for this work is libsim_iwbda.py. The gate library used

https://doi.org/10.1021/acssynbio.4c00438
ACS Synth. Biol. 2025, 14, 1425−1436

has been created by fitting the parameters in 4 to the ones of Cello's gate library.[10]

4.4. Regarding the Split-Transcript Approach. We briefly show in the following that under certain conditions, the steady state of the split-transcript approach can be approximated by the single-transcript eq 1, so that the results for the single transcript apply for the split-transcript under these conditions. Note that the strict stoichiometric relations are lost in the split-transcript approach, so that − while the ODE model is well approximated − stochastic computations will still be sensitive to this change.

4.4.1. Reaction Network of the Split-Transcript Feedback/Feedforward. The reactions involved in the split-transcript approach are more numerous than for the single transcript. Compared to Section 4.4.1, we applied the following changes. We first renamed the species' for the full RNA transcripts to M_{x+} and M_{y+}. Then, we added the partial RNA species' M_x and M_y that consist of the mRNA part only. Finally, we added the species W_x and W_y respresenting the asRNA part only. The species M_x, M_y, W_x, and W_y are produced by split reactions from the full transcript species M_{x+} and M_{y+}. We further assume that the splitting reaction happens with a sufficiently large rate, so that the full RNAs M_{x+} and M_{y+} are effectively not targeted by the corresponding asRNAs W_y or W_x and their degradation can be ignored. Given these changes and assumptions, the reactions for the split-transcript approach can be given as

$$X_{ON} \xrightarrow{\mu_1} X_{ON} + M_{x+} \qquad G_{ON} \xrightarrow{\mu_2} G_{ON} + M_{y+} \qquad M_x + W_x \xrightarrow{\delta_x} \varnothing$$

$$G_{OFF} \xrightarrow{\mu_{2,l}} G_{OFF} + M_{y+} \qquad M_{x+} \xrightarrow{\sigma_1} M_x + W_y \qquad M_y + W_y \xrightarrow{\delta_y} \varnothing$$

$$M_{x/y} \xrightarrow{\mu_P} M_{x/y} + P_{x/y} \qquad M_{y+} \xrightarrow{\sigma_2} M_y + W_x$$

and for the degradation reactions as

$$M_x \xrightarrow{\gamma_1} \varnothing \qquad W_x \xrightarrow{\omega_1} \varnothing \qquad P_{x/y} \xrightarrow{\gamma_P} \varnothing \qquad M_y \xrightarrow{\gamma_2} \varnothing \qquad W_y \xrightarrow{\omega_2} \varnothing$$

For this set of reactions, we can again require the QSS assumption 11. The resulting reaction rate equations are then

$$\frac{\mathrm{d}}{\mathrm{d}t}m_{x+} = \mu_1 x - \sigma_1 m_{x+} \qquad \frac{\mathrm{d}}{\mathrm{d}t}m_{y+} = \mu_2 \alpha_y - \sigma_2 m_{y+}$$

$$\frac{\mathrm{d}}{\mathrm{d}t}m_x = \sigma_1 m_{x+} - \gamma_1 m_x - \delta_x m_x w_x - \frac{\mathrm{d}}{\mathrm{d}t}m_y = \sigma_2 m_{y+} - \gamma_2 m_y - \delta_y m_y w_y$$

$$\frac{\mathrm{d}}{\mathrm{d}t}w_x = \sigma_2 m_{y+} - \omega_1 w_x - \delta_x m_x w_x - \frac{\mathrm{d}}{\mathrm{d}t}w_y = \sigma_1 m_{x+} - \omega_2 w_y - \delta_y m_y w_y$$

$$\frac{\mathrm{d}}{\mathrm{d}t}p_x = \mu_P m_x - \gamma_P p_x \qquad \frac{\mathrm{d}}{\mathrm{d}t}p_y = \mu_P m_y - \gamma_P p_y$$

with the new rate constants σ_1 and σ_2 for the split reactions and the degradation rates of the asRNA part species ω_1 and ω_2, and the separate sequestration rate constants δ_x and δ_y.

4.4.2. Approximation of the Split-Transcript by the Single-Transcript Approach. For the steady state, we can do the following simplification. First, we can see that in the steady state, the relations

$$m_x = \frac{(\omega_1 + \delta_x m_x)\sigma_1 m_{x+}}{(\omega_1 + \delta_x m_x)\gamma_1 + \delta_x \sigma_2 m_{y+}} \text{ and } w_y = \frac{(\gamma_2 + \delta_y w_y)\sigma_1 m_{x+}}{(\gamma_2 + \delta_y w_y)\omega_2 + \delta_y \sigma_2 m_{y+}} \tag{13}$$

hold. Two analoguous equations hold for m_y and w_x. These equations have two solutions and m_x and w_y can have up to two possible steady states. We will in the following show that for any given m_{x+} and m_{y+} there is only one valid pair (m_x, w_y). We now demonstrate the necessary calculations at the example of m_x. This can be seen by recognizing that we can rewrite 13 to obtain

$$m_x^2 + \underbrace{\left(\frac{\omega_1}{\delta_x} + \frac{\sigma_2}{\gamma_1}m_{y+} - \frac{\sigma_1}{\gamma_1}m_{x+}\right)}_{\equiv b} m_x - \frac{\omega_1 \sigma_1}{\delta_x \gamma_1} m_{x+} = 0$$

The discriminant $\Delta$of this quadratic equation tells us all we need to know about its possible solutions m_x. The discriminant satisfies

$$\Delta = \left(\frac{\sigma_2}{\gamma_1}m_{y+} - \frac{\sigma_1}{\gamma_1}m_{x+}\right)^2 + \text{pos.const.} = \left(\frac{\sigma_1}{\gamma_1}m_{x+} - \frac{\sigma_2}{\gamma_1}m_{y+}\right)^2 + \text{pos.const.} \geq 0$$

Thus, there are only real solutions for m_x and two of those by the number. To show that for any given m_{x+} and m_{y+} one solution is unreachable (and therefore only one remains), we need to demonstrate that always either

$$-b \leq -\sqrt{\Delta} \text{ or } -b \leq \sqrt{\Delta}$$

where we can assume that the *or* is mutually exclusive and we will concentrate on the second inequality. We first look at the case $\sigma_1 m_{x+} - \sigma_2 m_{y+} \geq 0$. There,

$$-\frac{\omega_1}{d_x} \leq 0 \Rightarrow -b \leq \sqrt{\Delta}$$

the solution $m_x = -b - \sqrt{\Delta}$ is not reachable (as $m_x \geq 0$). For the case $\sigma_2 m_{y+} - \sigma_1 m_{x+} \geq 0$, we simply have

$$\underbrace{2\left(\frac{\sigma_1}{\gamma_1}m_{x+} - \frac{\sigma_2}{\gamma_1}m_{y+}\right)}_{\leq 0} - \frac{\omega_1}{\delta_x} \leq 0 \Rightarrow -b \leq \sqrt{\Delta}$$

which guarantees us that for any given m_{x+} and m_{y+} there is only one valid corresponding m_x. Whether multiple pairs (m_{x+}, m_{y+}) are valid for one m_x is irrelevant, since they must be the same for m_x and w_y alike. This establishes a one-to-one correspondence of the possible steady states for m_x and w_y. We now consider the case $\delta_x = \delta_y \equiv \delta$. If the additional conditions $\gamma_1 \approx \omega_2$ and $\gamma_2 \approx \omega_1$ hold, then $m_x \approx w_y$ for the pairs (m_x, w_y). The analogue holds for the pairs (m_y, w_x), so that $m_y \approx w_x$ whenever $\gamma_2 \approx \omega_1$ and $\gamma_1 \approx \omega_2$ (the same conditions). As a final step, we can recognize that we may substitute

$$\sigma_1 m_{x+} = \mu_1 x \text{ and } \sigma_2 m_{y+} = \mu_2 \alpha_y$$

https://doi.org/10.1021/acssynbio.4c00438
ACS Synth. Biol. 2025, 14, 1425−1436

which lets us, as long as given assumptions and conditions are valid, consider the eq 1 a viable approximation for the split-transcript approach.

AUTHOR INFORMATION

Corresponding Author

Heinz Koeppl − *Department of Electrical Engineering and Information Technology and Centre for Synthetic Biology, TU Darmstadt, Darmstadt 64283, Germany*; Email: heinz.koeppl@tu-darmstadt.de

Authors

Nicolai Engelmann − *Department of Electrical Engineering and Information Technology, TU Darmstadt, Darmstadt 64283, Germany*; orcid.org/0000-0002-6318-7859

Maik Molderings − *Department of Electrical Engineering and Information Technology and Graduate School Life Science Engineering, TU Darmstadt, Darmstadt 64283, Germany*

Complete contact information is available at: https://pubs.acs.org/10.1021/acssynbio.4c00438

Author Contributions

N.E. provided mathematical analysis and programming. M.M. provided biological background. H.K. provided the idea. All authors contributed to the writing of this paper.

Funding

Funded by the European Union (ERC-PoC PLATE, GA 101082333). Views and opinions expressed are however those of the author(s) only and do not necessarily reflect those of the European Union. Neither the European Union nor the granting authority can be held responsible for them. Additionally M.M. was funded by the Deutsche Forschungsgemeinschaft (DFG, German Research Foundation) − project number 541299811.

Notes

The authors declare no competing financial interest.

The model is implemented as part of the technology mapping framework ARCTIC, which is available at https://www.rs.tu-darmstadt.de/ARCTIC.

ACKNOWLEDGMENTS

The authors thank Jérémie Marlhens and Erik Kubaczka for fruitful discussions and proof-reading.

REFERENCES

(1) Alon, U. *An introduction to systems biology: design principles of biological circuits*; CRC Press, 2019.

(2) Gardner, T. S.; Cantor, C. R.; Collins, J. J. Construction of a genetic toggle switch in Escherichia coli. *Nature* **2000**, *403*, 339−342.

(3) Cardinale, S.; Arkin, A. P. Contextualizing context for synthetic biology−identifying causes of failure of synthetic biological systems. *Biotechnology Journal* **2012**, *7*, 856−866.

(4) Brewster, R. C.; Weinert, F. M.; Garcia, H. G.; Song, D.; Rydenfelt, M.; Phillips, R. The Transcription Factor Titration Effect Dictates Level of Gene Expression. *Cell* **2014**, *156*, 1312−1323.

(5) Rydenfelt, M.; Cox, R. S., III; Garcia, H.; Phillips, R. Statistical mechanical model of coupled transcription from multiple promoters due to transcription factor titration. *Phys. Rev. E* **2014**, *89*, No. 012702.

(6) PMID: 36693176. Engelmann, N.; Schwarz, T.; Kubaczka, E.; Hochberger, C.; Koeppl, H. Context-Aware Technology Mapping in Genetic Design Automation. *ACS Synth. Biol.* **2023**, *12*, 446−459.

(7) Jeong, E. M.; Song, Y. M.; Kim, J. K. Combined multiple transcriptional repression mechanisms generate ultrasensitivity and oscillations. *Interface Focus* **2022**, *12*, 20210084.

(8) Brophy, J. A.; Voigt, C. A. Principles of genetic circuit design. *Nat. Methods* **2014**, *11*, 508−520.

(9) Buecherl, L.; Myers, C. J. Engineering genetic circuits: advancements in genetic design automation tools and standards for synthetic biology. *Curr. Opin. Microbiol.* **2022**, *68*, No. 102155.

(10) Nielsen, A. A.; Der, B. S.; Shin, J.; Vaidyanathan, P.; Paralanov, V.; Strychalski, E. A.; Ross, D.; Densmore, D.; Voigt, C. A. Genetic circuit design automation. *Science* **2016**, *352*, No. aac7341.

(11) Chen, Y.; Zhang, S.; Young, E. M.; Jones, T. S.; Densmore, D.; Voigt, C. A. Genetic circuit design automation for yeast. *Nature Microbiology* **2020**, *5*, 1349−1360.

(12) Xie, M.; Fussenegger, M. Designing cell function: assembly of synthetic gene circuits for cell biology applications. *Nat. Rev. Mol. Cell Biol.* **2018**, *19*, 507−525.

(13) Chappell, J.; Takahashi, M. K.; Meyer, S.; Loughrey, D.; Watters, K. E.; Lucks, J. The centrality of RNA for engineering gene expression. *Biotechnology Journal* **2013**, *8*, 1379−1395.

(14) Schmidt, C. M.; Smolke, C. D. RNA switches for synthetic biology. *Cold Spring Harbor Perspectives in Biology* **2019**, *11*, No. a032532.

(15) Dykstra, P. B.; Kaplan, M.; Smolke, C. D. Engineering synthetic RNA devices for cell control. *Nat. Rev. Genet.* **2022**, *23*, 215−228.

(16) Lehr, F.-X.; Hanst, M.; Vogel, M.; Kremer, J.; Göringer, H. U.; Suess, B.; Koeppl, H. Cell-free prototyping of AND-logic gates based on heterogeneous RNA activators. *ACS Synth. Biol.* **2019**, *8*, 2163−2173.

(17) Green, A. A.; Silver, P. A.; Collins, J. J.; Yin, P. Toehold switches: de-novo-designed regulators of gene expression. *Cell* **2014**, *159*, 925−939.

(18) Zhao, E. M.; Mao, A. S.; de Puig, H.; Zhang, K.; Tippens, N. D.; Tan, X.; Ran, F. A.; Han, I.; Nguyen, P. Q.; Chory, E. J.; et al. RNA-responsive elements for eukaryotic translational control. *Nat. Biotechnol.* **2022**, *40*, 539−545.

(19) Bartoli, V.; Meaker, G. A.; Di Bernardo, M.; Gorochowski, T. E. Tunable genetic devices through simultaneous control of transcription and translation. *Nat. Commun.* **2020**, *11*, 2095.

(20) Bartoli, V.; di Bernardo, M.; Gorochowski, T. E. Self-adaptive biosystems through tunable genetic parts and circuits. *Current Opinion in Systems Biology* **2020**, *24*, 78−85.

(21) Laurent, G. S.; Wahlestedt, C.; Kapranov, P. The Landscape of long noncoding RNA classification. *Trends Genet.* **2015**, *31*, 239−251.

(22) Hammond, S. M. An overview of microRNAs. *Adv. Drug Delivery Rev.* **2015**, *87*, 3−14.

(23) Holmqvist, E.; Unoson, C.; Reimegård, J.; Wagner, E. G. H. A mixed double negative feedback loop between the sRNA MicF and the global regulator Lrp. *Molecular microbiology* **2012**, *84*, 414−427.

(24) Tu, K. C.; Long, T.; Svenningsen, S. L.; Wingreen, N. S.; Bassler, B. L. Negative feedback loops involving small regulatory RNAs precisely control the Vibrio harveyi quorum-sensing response. *Molecular cell* **2010**, *37*, 567−579.

(25) Marciano, D. C.; Lua, R. C.; Katsonis, P.; Amin, S. R.; Herman, C.; Lichtarge, O. Negative feedback in genetic circuits confers evolutionary resilience and capacitance. *Cell reports* **2014**, *7*, 1789−1795.

(26) Levine, E.; Zhang, Z.; Kuhlman, T.; Hwa, T. Quantitative characteristics of gene regulation by small RNA. *PLoS biology* **2007**, *5*, No. e229.

(27) Frei, T.; Chang, C.-H.; Filo, M.; Arampatzis, A.; Khammash, M. A genetic mammalian proportional−integral feedback control circuit for robust and precise gene regulation. *Proc. Natl. Acad. Sci. U. S. A.* **2022**, *119*, No. e2122132119.

(28) Meister, G.; Tuschl, T. Mechanisms of gene silencing by double-stranded RNA. *Nature* **2004**, *431*, 343−349.

(29) Kay, C.; Skotte, N.; Southwell, A.; Hayden, M. Personalized gene silencing therapeutics for Huntington disease. *Clinical Genetics* **2014**, *86*, 29−36.

(30) Obbard, D. J.; Gordon, K. H.; Buck, A. H.; Jiggins, F. M. The evolution of RNAi as a defence against viruses and transposable elements. *Philosophical Transactions of the Royal Society B: Biological Sciences* **2009**, *364*, 99−115.
(31) Verd, B.; Crombach, A.; Jaeger, J. Classification of transient behaviours in a time-dependent toggle switch model. *BMC systems biology* **2014**, *8*, 1−19.
(32) Bernhart, S. H.; Tafer, H.; Mückstein, U.; Flamm, C.; Stadler, P. F.; Hofacker, I. L. Partition function and base pairing probabilities of RNA heterodimers. *Algorithms Mol. Biol.* **2006**, *1*, 3.
(33) Gander, M. W.; Vrana, J. D.; Voje, W. E.; Carothers, J. M.; Klavins, E. Digital logic circuits in yeast with CRISPR-dCas9 NOR gates. *Nat. Commun.* **2017**, *8*, No. 15459.
(34) Tamsir, A.; Tabor, J. J.; Voigt, C. A. Robust multicellular computing using genetically encoded NOR gates and chemical 'wires'. *Nature* **2011**, *469*, 212−215.
(35) Goñi-Moreno, A.; Amos, M. A reconfigurable NAND/NOR genetic logic gate. *BMC Syst. Biol.* **2012**, *6*, 126.
(36) Park, Y.; Espah Borujeni, A.; Gorochowski, T. E.; Shin, J.; Voigt, C. A. Precision design of stable genetic circuits carried in highly-insulated E. coli genomic landing pads. *Mol. Syst. Biol.* **2020**, *16*, No. e9584.
(37) Miyamoto, T.; Razavi, S.; DeRose, R.; Inoue, T. Synthesizing biomolecule-based Boolean logic gates. *ACS Synth. Biol.* **2013**, *2*, 72−82.
(38) Manzoni, R.; Urrios, A.; Velazquez-Garcia, S.; de Nadal, E.; Posas, F. Synthetic biology: insights into biological computation. *Integrative Biology* **2016**, *8*, 518−532.
(39) Ferrell, J. E.; Ha, S. H. Ultrasensitivity part I: Michaelian responses and zero-order ultrasensitivity. *Trends Biochem. Sci.* **2014**, *39*, 496−503.
(40) Ferrell, J. E.; Ha, S. H.; et al. Ultrasensitivity part II: multisite phosphorylation, stoichiometric inhibitors, and positive feedback. *Trends Biochem. Sci.* **2014**, *39*, 556−569.
(41) Ferrell, J. E.; Ha, S. H. Ultrasensitivity part III: cascades, bistable switches, and oscillators. *Trends Biochem. Sci.* **2014**, *39*, 612−618.
(42) Jeong, E. M.; Kim, J. K. A robust ultrasensitive transcriptional switch in noisy cellular environments. *npj Syst. Biol. Appl.* **2024**, *10*, 30.
(43) Kafri, M.; Metzl-Raz, E.; Jona, G.; Barkai, N. The cost of protein production. *Cell Reports* **2016**, *14*, 22−31.
(44) Rosenfeld, N.; Alon, U. Response delays and the structure of transcription networks. *J. Mol. Biol.* **2003**, *329*, 645−654.
(45) Singh, I. K.; Singh, S.; Mogilicherla, K.; Shukla, J. N.; Palli, S. R. Comparative analysis of double-stranded RNA degradation and processing in insects. *Sci. Rep.* **2017**, *7*, 17059.
(46) Wang, Q.; Carmichael, G. G. Effects of length and location on the cellular response to double-stranded RNA. *Microbiology and Molecular Biology Reviews* **2004**, *68*, 432−452.
(47) Wery, M.; Descrimes, M.; Vogt, N.; Dallongeville, A.-S.; Gautheret, D.; Morillon, A. Nonsense-mediated decay restricts LncRNA levels in yeast unless blocked by double-stranded RNA structure. *Mol. Cell* **2016**, *61*, 379−392.
(48) Bayer, T. S.; Smolke, C. D. Programmable ligand-controlled riboregulators of eukaryotic gene expression. *Nat. Biotechnol.* **2005**, *23*, 337−343.
(49) Briat, C.; Gupta, A.; Khammash, M. Antithetic integral feedback ensures robust perfect adaptation in noisy biomolecular networks. *Cell Systems* **2016**, *2*, 15−26.
(50) Specht, D. A.; Cortes, L. B.; Lambert, G. Overcoming leak sensitivity in CRISPRi circuits using antisense RNA sequestration and regulatory feedback. *ACS Synth. Biol.* **2022**, *11*, 2927−2937.
(51) Guet, C. C.; Elowitz, M. B.; Hsing, W.; Leibler, S. Combinatorial synthesis of genetic networks. *Science* **2002**, *296*, 1466−1470.
(52) Bintu, L.; Buchler, N. E.; Garcia, H. G.; Gerland, U.; Hwa, T.; Kondev, J.; Phillips, R. Transcriptional regulation by the numbers: models. *Current Opinion in Genetics & Development* **2005**, *15*, 116−124.
(53) Schile, A. J.; Limmer, D. T. Rate constants in spatially inhomogeneous systems. *J. Chem. Phys.* **2019**, *150*, 191102.
(54) Mano, M. M.; Ciletti, M. D. *Digital Design*; Pearson Education, 2002.
(55) Steininger, A.; Maier, J.; Najvirt, R. The metastable behavior of a schmitt-trigger. In *2016 22nd IEEE International Symposium on Asynchronous Circuits and Systems (ASYNC)*, 2016; pp 57−64.
(56) Yoo, S. M.; Na, D.; Lee, S. Y. Design and use of synthetic regulatory small RNAs to control gene expression in Escherichia coli. *Nature protocols* **2013**, *8*, 1694−1707.
(57) Schladt, T.; Engelmann, N.; Kubaczka, E.; Hochberger, C.; Koeppl, H. Automated design of robust genetic circuits: Structural variants and parameter uncertainty. *ACS Synth. Biol.* **2021**, *10*, 3316−3329.
(58) Schwarz, K. E. A. Engelmann ARCTIC Design Automation Toolchain, 2021. https://gitlab.rs.e-technik.tu-darmstadt.de/arctic/arctic.
(59) Hoynes-O'Connor, A.; Moon, T. S. Development of design rules for reliable antisense RNA behavior in E. coli. *ACS synthetic biology* **2016**, *5*, 1441−1454.
(60) Ren, J.; Nong, N. T.; Lam Vo, P. N.; Lee, H.-M.; Na, D. Rational Design of High-Efficiency Synthetic Small Regulatory RNAs and Their Application in Robust Genetic Circuit Performance Through Tight Control of Leaky Gene Expression. *ACS Synth. Biol.* **2024**, *13*, 3256−3267.
(61) Bloom, R. J.; Winkler, S. M.; Smolke, C. D. A quantitative framework for the forward design of synthetic miRNA circuits. *Nat. Methods* **2014**, *11*, 1147−1153.
(62) Matsuura, S.; Ono, H.; Kawasaki, S.; Kuang, Y.; Fujita, Y.; Saito, H. Synthetic RNA-based logic computation in mammalian cells. *Nat. Commun.* **2018**, *10*, 1950.
(63) Solodushko, V.; Fouty, B. Terminal hairpins improve protein expression in IRES-initiated mRNA in the absence of a cap and polyadenylated tail. *Gene Ther.* **2023**, *30*, 620−627.
(64) Lee, Y.; Ahn, C.; Han, J.; Choi, H.; Kim, J.; Yim, J.; Lee, J.; Provost, P.; Rådmark, O.; Kim, S.; et al. The nuclear RNase III Drosha initiates microRNA processing. *Nature* **2003**, *425*, 415−419.
(65) Hussein, R.; Lim, H. N. Disruption of small RNA signaling caused by competition for Hfq. *Proc. Natl. Acad. Sci. U. S. A.* **2011**, *108*, 1110−1115.
(66) Peng, H.; Latifi, B.; Müller, S.; Lupták, A.; Chen, I. A. Self-cleaving ribozymes: substrate specificity and synthetic biology applications. *RSC chemical biology* **2021**, *2*, 1370−1383.
(67) Zand, A. M.; Gupta, A.; Khammash, M. *Cascaded antithetic integral feedback for enhanced stability and performance*; IEEE Control Systems Letters, 2024.
(68) Zhu, R.; del Rio-Salgado, J. M.; Garcia-Ojalvo, J.; Elowitz, M. B. Synthetic multistability in mammalian cells. *Science* **2022**, *375*, No. eabg9765.
(69) Kordyś, M.; Sen, R.; Warkocki, Z. Applications of the versatile CRISPR-Cas13 RNA targeting system. *Wiley Interdiscip. Rev.: RNA* **2022**, *13*, No. e1694.
(70) Özcan, A.; Krajeski, R.; Ioannidi, E.; Lee, B.; Gardner, A.; Makarova, K. S.; Koonin, E. V.; Abudayyeh, O. O.; Gootenberg, J. S. Programmable RNA targeting with the single-protein CRISPR effector Cas7−11. *Nature* **2021**, *597*, 720−725.
(71) Huang, L.; Yuan, Z.; Liu, P.; Zhou, T. Effects of promoter leakage on dynamics of gene expression. *BMC Syst. Biol.* **2015**, *9*, 16.

https://doi.org/10.1021/acssynbio.4c00438
ACS Synth. Biol. 2025, 14, 1425−1436